DOI: 10.1002/cplu.201402007

Catalytic Performance of Vanadium MIL-47 and Linker-Substituted Variants in the Oxidation of Cyclohexene: A Combined Theoretical and Experimental Approach

Matthias Vandichel,*[a] Shyam Biswas,[b] Karen Leus,[b] Joachim Paier,[c] Joachim Sauer,[c] Toon Verstraelen,[a] Pascal Van Der Voort,*[b] Michel Waroquier,*[a] and Veronique Van Speybroeck*[a]

The epoxidation of cyclohexene has been investigated on a metal–organic framework MIL-47 containing saturated V^{+IV} sites linked with functionalized terephthalate linkers (MIL-47-X, X = OH, F, Cl, Br, CH_3, NH_2). Experimental catalytic tests have been performed on the MIL-47-X materials to elucidate the effect of linker substitution on the conversion. Notwithstanding the fact that these substituted materials are prone to leaching in the performed catalytic tests, the initial catalytic activity of these materials correlates with the Hammett substituent constants. In general, substituents led to an increased activity relative to the parent MIL-47. To rationalize the experimental findings, first-principles kinetic calculations were performed on periodic models of MIL-47 to determine the most important active sites by creating defect structures in the interior of the crystalline material. In a next step these defect structures were used to propose extended cluster models, which are able to reproduce in an adequate way the direct environment of the active metal site. An alkylperoxo species $V^{+V}O(OOtBu)$ was identified as the most abundant and therefore the most active epoxidation site. The structure of the most active site was a starting basis for the construction of extended cluster models including substituents. They were used for quantifying the effect of functionalization of the linkers on the catalytic performance of the heterogeneous catalyst MIL-47-X. Electron-withdrawing as well as electron-donating groups have been considered. The epoxidation activity of the functionalized models has been compared with the measured experimental conversion of cyclohexene. The agreement is fairly good. This combined experimental–theoretical study makes it possible to elucidate the structure of the most active site and to quantify the electronic modulating effects of linker substituents on the catalytic activity.

Introduction

Over the past decade, metal–organic frameworks (MOFs) have emerged as an important new class of nanoporous materials and can be considered as the most recent development and challenge in the field of ordered porous materials.[1] This new class of porous materials has a truly hybrid character, since both inorganic and organic moieties are necessary to build up the framework. In this way, MOFs can provide a bridge between organic polymers and inorganic crystalline zeolites and are sometimes also referred to as a crystalline subclass within the porous coordination polymers. Since the 1990s, this area of chemistry has experienced an almost unparalleled growth, witnessed not only by the large number of research and review papers published but also by the ever-expanding scope of the research.[2] MOFs have been reviewed both from a general perspective[1,3] and as more application-related. For example, MOFs have been studied extensively for adsorption and gas storage,[4] separation,[5] catalysis,[6] optics and sensing,[7] and electrical/magnetic properties.[8] Recently, MOFs have also been examined for biomedical applications such as controlled drug delivery.[9]

In view of the broad variety of applications, more and more attempts have been made to tune the properties of MOFs at the nanoscale level. Various studies have been published on the functionalization of the organic linkers without altering the original topology of the material. A class of MOFs that can be regarded as a prototype of nanoporous materials, in which pore size and functionality on the organic linker can be varied systematically without changing the topology, is MOF-5. It is constructed from octahedral Zn–O–C clusters and benzene linkers, and its three-dimensional pore system can be functionalized with the organic groups Br, NH_2, OC_3H_7, OC_5H_{11}, and

[a] Dr. M. Vandichel, Prof. T. Verstraelen, Prof. M. Waroquier, Prof. V. Van Speybroeck
Center for Molecular Modeling
Universiteit Gent, Technologiepark 903, 9052 Zwijnaarde (Belgium)
E-mail: Matthias.Vandichel@Ugent.be
Michel.Waroquier@Ugent.be
Veronique.VanSpeybroeck@Ugent.be

[b] Dr. S. Biswas, Dr. K. Leus, Prof. P. Van Der Voort
COMOC—Centre for Ordered Materials, Organometallics and Catalysis
Universiteit Gent, Krijgslaan 281-S3, 9000 Gent (Belgium)
E-mail: Pascal.VanDerVoort@Ugent.be

[c] Dr. J. Paier, Prof. J. Sauer
Institut für Chemie, Humboldt-Universität zu Berlin
Unter den Linden 6, 10099 Berlin (Germany)

Supporting information for this article is available on the WWW under http://dx.doi.org/10.1002/cplu.201402007.

C_2H_4.[10] Another example is presented in the work of Serra-Crespo et al., in which a pure phase amine-functionalized MIL-101(Al) was synthesized and found to be an excellent candidate for the selective adsorption of CO_2 from methane and N_2.[11] Various studies on the substituted versions of MIL-53(M) with M = Cr,[12] Fe,[13] Al,[14] and Sc[15] are also highly interesting, as they have shown different adsorption isotherms and breathing behavior. The influence of functionalization was particularly explored for sorption and separation studies of molecules such as CO_2, CH_4, and so forth. Recently, the UiO-66-X series was investigated for both CO_2/CH_4 separation and catalysis. Grand canonical Monte Carlo calculations showed that SO_3H- and CO_2H-functionalized materials exhibit the highest selectivity for CO_2/CH_4 separation.[16] With respect to catalysis, some of the present authors have shown a remarkable influence of electronic linker modulations of the UiO-66 (UiO-66-X) material on the catalytic activity for the citronellal cyclization.[17] Functionalized linkers could greatly enhance the catalytic performance of the coordinatively unsaturated Lewis acid sites. Nitro-group substitution resulted in a 56-fold increase in rate. This effect was confirmed by theoretical modeling on a well-chosen defect site, and resulted in a substantial lowering of both the apparent and intrinsic free-energy barrier.

MOFs have also been explored as heterogeneous catalysts for oxidation reactions using peroxides or molecular oxygen as oxidant. An excellent review on this item was recently presented by Garcia and co-workers.[6b] Heterogeneous catalytic oxidation reactions were also investigated in Co-MOFs (MFU-1 and MFU-2).[18] The liquid-phase oxidation of cyclohexene, employing *tert*-butyl hydroperoxide (TBHP) as oxidant, has been investigated and for both MOFs large conversions of cyclohexene were noticed. Although MFU-1 performed as a truly heterogeneous and robust catalyst, MFU-2 suffered from metal leaching into solution. In a previous study of some of the authors,[19] the same oxidation reaction has been studied over a coordinatively saturated vanadium-MOF: V-MIL-47. Apart from cyclohexene oxide **2**, the product distribution consisted of the consecutively formed cyclohexane-1,2-diol **3** and (radical) side products *tert*-butyl-2-cyclohexenyl-1-peroxide **4** and cyclohexen-2-one **5** (Figure 1 a). The catalyst is believed to act partly heterogeneously, which was confirmed by hot filtration experiments.[19] After hot filtration of the catalyst, the conversion towards the epoxide almost stops while the radical products are still formed. This could be a result of 1) the presence of radical pathways that are also able to produce epoxide[20] and 2) leached V sites in solution.[21] In a recent theoretical study, we performed a complete mechanistic investigation of the possible epoxidation pathways for the homogeneous VO(acac)$_2$ (acac = acetylacetonate) system.[21] The concerted Sharpless mechanism turned out to be preferred and the alkylperoxo species $V^{+V}O(L_1)(L_2)(OOtBu)$ (with L_1, L_2 = OH, acac, acetate (OAc), and *tert*-butoxide anion (O*t*Bu)) were proposed as the most active sites in the epoxidation of cyclohexene.

The aim of this study is twofold. First, the effects of linker substitution on the epoxidation performance of the vanadium catalyst MIL-47 are studied in a combined experimental–computational effort. Modifications with both electron-withdrawing (OH, F, Cl, Br) and electron-donating (CH_3, NH_2) groups are investigated. To the best of our knowledge the functionalized

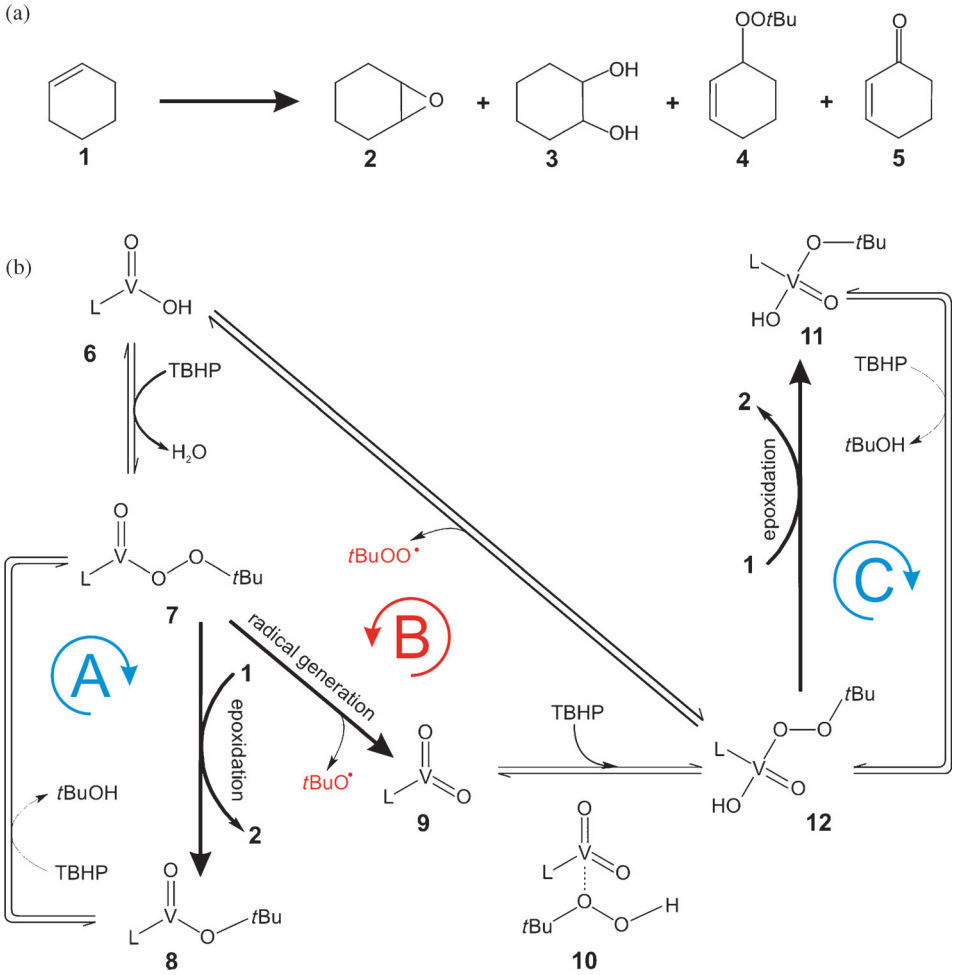

Figure 1. a) Oxidation of cyclohexene **1** to cyclohexene oxide **2** and the consecutive ring opening to cyclohexane-1,2-diol **3**, *tert*-butyl-2-cyclohexenyl-1-peroxide **4**, and allylic oxidation to 2-cyclohexene-1-one **5**. b) Two competitive cyclohexene epoxidation pathways (**7**→**8** and **12**→**11**) and radical generation reactions (**7**→**9** and **12**→**6**) allow the transformation of oxidation state from +IV to +V and vice versa. L represents the two terephthalate ligands to which the vanadyl oxygen atoms coordinate.

MIL-47-X series has not been studied before for this purpose. Second, special attention is devoted to the methodology (cluster versus periodic approaches) to describe the structure of the most active catalytic sites in MIL-47. The MIL-47 structure consists of a three-dimensional framework, in which each V^{+IV} center is coordinated to four oxygen atoms from four different carboxylate groups and two oxygen atoms from the vanadyl V=O–V=O chain. As such, vanadium is fully saturated in an octahedral coordination mode.

The main catalytic pathways that have been modeled in our previous study[20] are shown in Figure 1 b. The reaction cycle starts with an activation step, in which the oxidant TBHP coordinates with the vanadium center to form an alkylperoxo species **7**. First, a direct epoxidation pathway may lead to the formation of cyclohexene oxide **2** and brings the catalyst to a less active complex **8**. Second, a radical mechanism is plausible (**7**→**9** in Figure 1 b). In this route V^{+V} vanadium complexes **9** are formed by homolytic cleavage of the peroxo linkage, which can then be further activated with TBHP. The generated V^{+V} activated complexes **10** and **12** can again epoxidize cyclohexene. Both direct epoxidations (A and C) and radical (B) routes are completed by a regeneration step, which closes the cycle by reducing the oxidation state +V back to +IV (Figure 1 b). Many more reactive pathways can occur through the catalytic cycle but the considered pathways here are selected as a proof of principle to determine an accurate catalyst model and investigate the influence of linker substitution. A complete overview of all possible epoxidation pathways can be found in our earlier study on $VO(acac)_2$.[21] The epoxidation reactions (**7**→**8**, **10**→**11**, **12**→**11**) and radical generation reactions (**7**→**9**, **12**→**6**) were described previously with the help of extended cluster models[20] (Figure 1 b). In this study, the reaction **10**→**11** was omitted, as it requires a higher free-energy barrier. It is more likely that complex **10** would react further to give complex **12**, thereby forming an active V^{+V} epoxidation species.

Herein, the creation of defect structures—required for making a vanadium site catalytically active—is investigated taking into account adequately the molecular environment. For this purpose, the methodology for a theoretical investigation of epoxidation reactions has been extended. In the search for the most appropriate active site, the reactions have been modeled in their most natural molecular environment. Undoubtedly, such a description is best provided by periodic models. They include a larger part of the environment of the active site than cluster models, and hence describe much better geometrical and electronic effects. Furthermore, periodic models give a significant added value to the discussion, as they provide extra insight into the epoxidation behavior of the MIL-47 catalyst, which is of primary importance to identify the exact nature of the active site. Once the structure of the most active site is determined by the periodic calculations, a cluster model can be constructed, which exhibits the same features of the active metal site as in the periodic model. Extended cluster calculations are computationally less demanding and therefore of high utility as a viable alternative for periodic calculations. The extracted cluster structure can be further used as starting basis for the construction of substituted MIL-47-X cluster models. As experimental data on cyclohexene conversion in functionalized MIL-47-X as catalysts are still missing in the literature, these materials were also synthesized in the frame of the goal of this study. The catalytic performance of these materials was investigated and compared carefully with the catalytic activity of the parent MIL-47. The combined theoretical and experimental approach will give us insight into the electronic modulation and its effect on the epoxidation mechanism of substituted MIL-47 materials.

Results and Discussion

Defects and active sites in MIL-47 materials: theoretical insight

Periodic model: creation of defects

In an undamaged fully saturated MIL-47 framework, the coordination sphere around vanadyl $[V{=}O]^{2+}$ is completely blocked by terephthalate linkers, which leaves no free position for substrate chemisorption or reactions. The catalytic activity of the material in the cyclohexene epoxidation with TBHP can only be started up by the presence of structural defects, thus making the vanadium sites available for reaction with TBHP and cyclohexene. These defects can be present at the surface of the material, but they can also be generated in the interior of the material by removal of at least two terephthalic acid (TA) molecules that are both connected to the same vanadium center. To study defect formation in a realistic molecular environment, it is mandatory to use periodic calculations that take into account the full crystalline environment of the defect. Additionally, such calculations enable us to evaluate the energy required for the creation of the various defects. The procedure followed to induce defects in the interior of the material and thus create active metal sites in the pores is outlined in Figure 2 and is as follows. First, the terephthalate linker is removed by interacting with water. Terephthalic acid (TA) is repelled and in the crystal replaced by terminating hydroxyl groups (this step is easily visualized in the top of Figure 2). Then, a second linker, connected to the same metal site, is also cut. Actually, there are two TA linkers that are candidates to be removed: they are highlighted with red tubes in the second row of Figure 2 (note that Figure 2 displays unit cells) and lead to defects of type A or B. The removal of a second terephthalate linker requires a substantially lower energy than the 227 kJ mol^{-1} free reaction energy needed to break up the first TA linker. The defect of type A appears to be energetically favored owing to a beneficial entropic contribution. In principle, there is now sufficient space to allow the TBHP oxidant and the cyclohexene substrate to come close to the vanadium site: a first active site has been created in the interior of the material. In reality it is not excluded that a vanadium site can be leached in solution and driven away from the crystal. This leaching process is indeed observed experimentally.[20,21] It is highly realistic that such defect structures actually occur in the interior of the material. The diagrams at the bottom of Figure 2 visualize two distinct vanadium centers that are removed, thus leaving the material in a disjointed structure. The

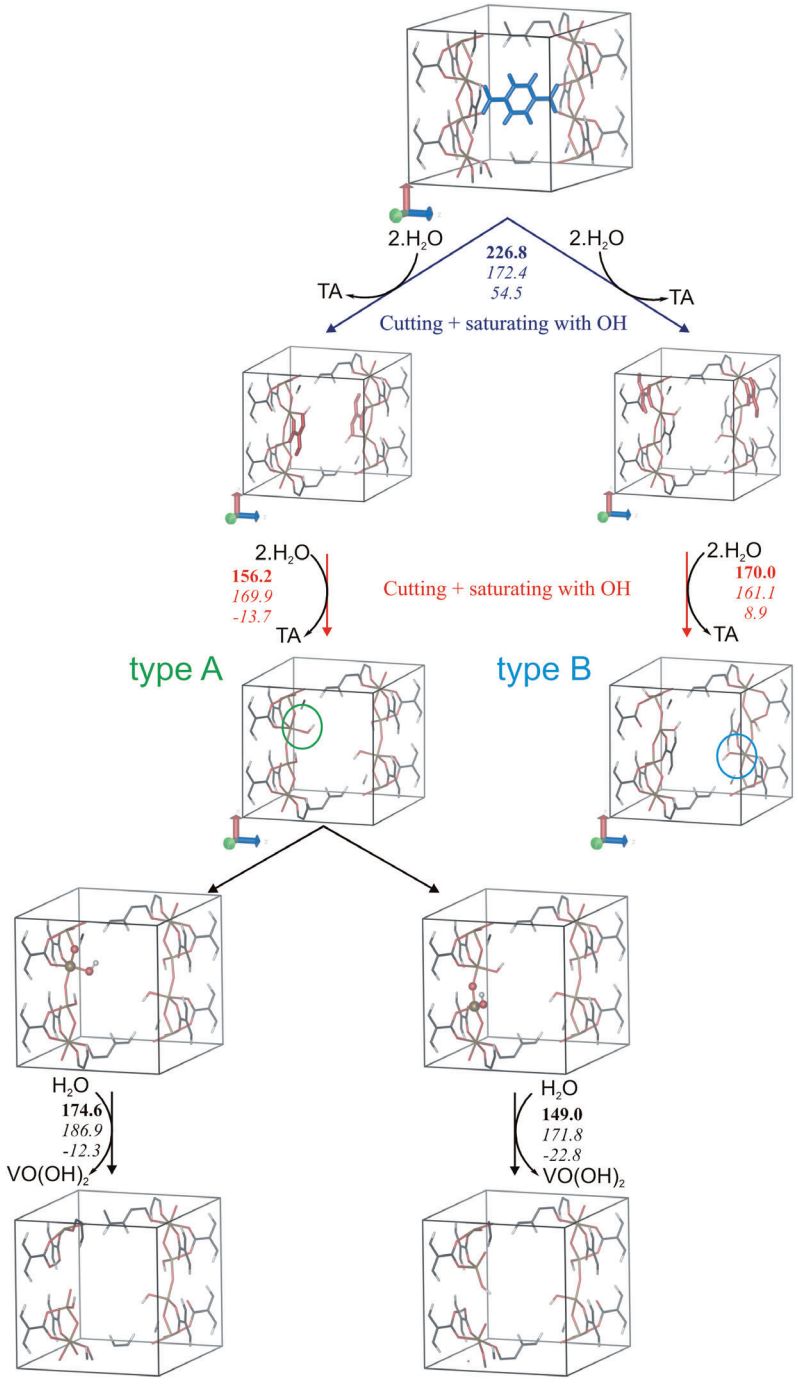

Figure 2. Consecutive removal of terephthalic linkers (TA) with water, starting from an undamaged unit cell (top). In the first step the TA linker highlighted with blue tubes has been removed. In the second step a second linker is cut (highlighted with red tubes). The two possibilities are visualized in the two middle figures. Note that periodic unit cells are represented, and to get a global picture of the induced defect in the interior of the material one should imagine the periodic images at each side of the unit cell. The free reaction energy is also given in kJ mol^{-1} together with its enthalpic and entropic contributions.

energy cost for the creation of defect structures is given in Figure 2. The required free energies are reasonable. At 323 K the cost is limited to 156 kJ mol^{-1} for the removal of the second TA linker and 149 kJ mol^{-1} for the removal of a vanadium site $VO(OH)_2$. A more realistic theoretical model would be the consideration of a 2×2×2 supercell consisting of at least eight unit cells. In this way the defect structure would be better embedded in the material and well isolated from the other defects.

With the above cutting procedure, large parts of the material can be leached creating large holes in the interior of the crystal. An estimate of the requested energy cost to achieve such a defect model is also given. A description of these defects requests large supercells, which make their use in further applications (e.g., simulation of chemical reactions in the pores) almost unfeasible owing to large computational costs. More realistic is the introduction of a periodic slab model. It mimics as well the active sites present at the outer surface of the material as the inner surface of the holes in the material. The proposed periodic slab model is created by cutting two TA linkers and two vanadyl groups from the optimized 2×1×1 MIL-47 supercell (Figure 3). The defects were taken parallel with the 100 crystal plane according to the crystallographic information file provided by Barthelet et al.[22] The way defects can be created is not unique, and we can distinguish between two different structures of open metal sites depending on how the linkers and vanadyl groups have been removed: removal of two TA linkers and two vanadyl groups enclosed in the blue rectangle (see Figure 3) leads to an active site of type I, whereas an active site of type II is characterized by removing the linkers and vanadium enclosed in the red rectangle. Water is added to satisfy the stoichiometry of the leaching reaction: the two unsaturated vanadium atoms at the end of the vanadyl chain are terminated with OH groups, thus maintaining the +IV oxidation state for the vanadium atoms. Additionally, to act as possible active metal sites occurring at the surface of the material or at the surface of large holes in the material, we incorporate a vacuum layer in the model to prevent artificial interactions between the terminal hydroxyl groups and the interrupted vanadyl chain. In this way we dispose of

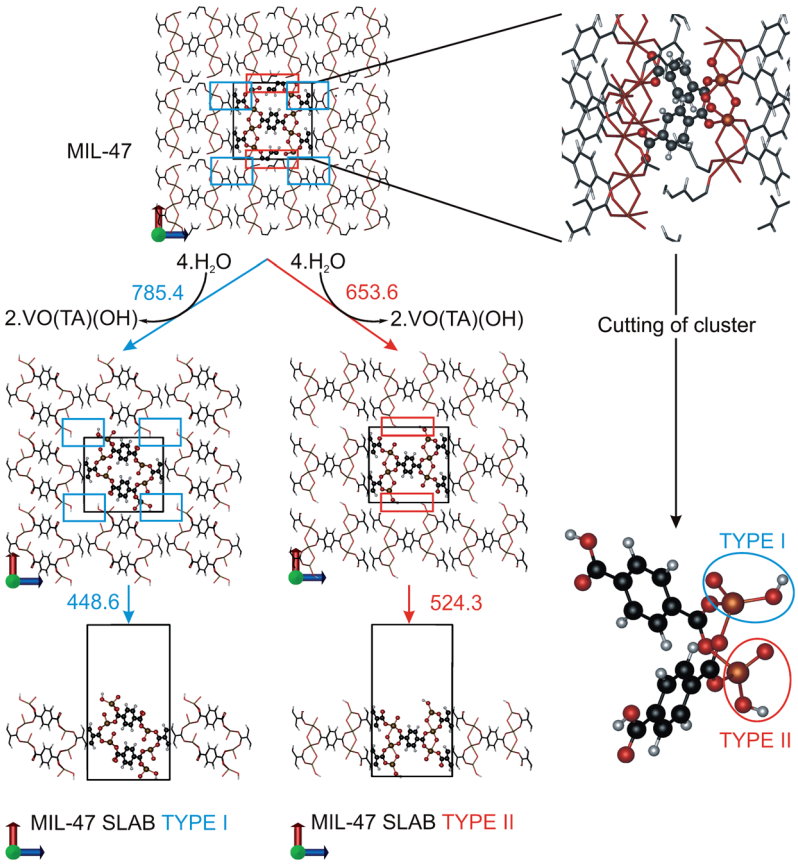

Figure 3. Removal of two terephthalic linkers (TA) and two vanadyl groups with water, starting from an undamaged unit cell (top). They are removed from two distinct positions in the crystal, denoted by blue and red rectangles, which lead to two different reaction sites I and II. The formation energy of the defect (at 0 K) is also given in kJ mol^{-1}.

two structurally different periodic slab models. The periodic slab of type II was found to be around 66 kJ mol^{-1} more stable than the slab of type I. As two defect sites are present in each periodic slab, this difference amounts to 33 kJ mol^{-1} per active site. This can probably be ascribed to some extra interaction between the terminating vanadyl oxygen and the saturating hydrogen terminating the carboxyl group in the case of MIL-47 slab type II (Figure 3).

Periodic model: reactivity for cyclohexene oxidation

In this section the activity of the constructed defect sites for cyclohexene oxidation is investigated. The reaction kinetics of the three main reactions **7**→**8**, **7**→**9**, and **12**→**11** in respective catalytic cycles A, B, and C (Figure 1) have been calculated in the periodic model. Computational details are given in the Experimental Section (see below). Only apparent energy and free-energy barriers (at 323 K) are presented in Table 1; for completeness all the other results are given in the Supporting Information (Tables S4 and S5). In these particular cases we understand under apparent kinetics that cyclohexene is handled in the gas phase as well as the product after the epoxidation. Following the results reported in Table 1 the direct epoxidation reaction **7**→**8** on type I defect sites is unlikely to compete with the faster radical generation **7**→**9** on the basis of the huge differences in free-energy barrier (101.9 versus 32.8 kJ mol^{-1}). Note also that the radical generation reaction **7**→**9** is unimolecular and that the lack of entropic contributions makes that energy and the Gibbs free-energy barrier close to each other (Table 1). This reaction is by far the most favorable reaction path starting from an active V^{+IV} alkylperoxo species. Usage of the PBE functional confirms the same qualitative trend (Table S5), but the absolute values deviate a lot. PBE predictions for apparent barriers are mostly underestimated,[18,23] which is typical for generalized gradient approximation-type functionals[24] even with inclusion of the semiempirical correction for dispersion. PBE0 is much more reliable for chemical kinetics, and can best be compared with values predicted by other hybrid functionals, such as B3LYP. For this reason we only retain the PBE0-D2 results for further assessment and comparison with the extended cluster calculations. We do not have the intention to repeat here the mechanism of the whole cyclohexene oxidation process with TBHP in MIL-47; it has been outlined in the Introduction and discussed extensively in reference [21]. We only stress the importance of the three main reactions we take into consideration, as they govern the whole catalytic cycle: the epoxidation reactions starting from V^{+IV} vanadium complexes, those starting from V^{+V} vanadium complexes, and the radical generation reactions transforming V^{+IV} to V^{+V}. The regeneration step **12**→**6** bringing a V^{+V} complex back to oxidation state +IV requires a reaction free energy of some 70 kJ mol^{-1} [21] and closes the catalytic cycle. Taking into account that all reaction steps are irreversible, the rate-determining step is the epoxidation step from an active V^{+V} complex. Regardless of the level of theory or type of active site, our results on the periodic slab model show that the radical generation reaction **7**→**9** is the fastest, followed by the epoxidation on a vanadium +IV site **7**→**8**, and that **12**→**11** is the slowest reaction. Periodic calculations seem to prefer type II active sites for the epoxidation reactions, but the energy differences of a few kJ mol^{-1} are such that we may not exclude active catalytic centers of type I in an overall assessment.

Simulations on active sites in the interior of the material (type A and B, Figure 2) are also instructive. The low apparent barrier of 14.7 kJ mol^{-1}, observed for the **7**→**8** epoxidation reaction at a vanadium center of type B, largely deviates from

Table 1. Apparent energy $\Delta E^{\neq}_0$ [kJ mol^{-1}] and free-energy barrier $\Delta G^{\neq}_{323}$ [kJ mol^{-1}] for the epoxidation reactions **7**→**8** and **12**→**11** in catalytic cycles A and C, respectively. Path **7**→**9** represents the competitive radical generation reaction V^{+IV}→V^{+V}.

Energy	7→8	7→9	12→11	7→8	7→9	12→11
	a) Periodic calculations (PBE0-D2) with defects in interior					
		Type A			Type B	
$\Delta E^{\neq}_0$	−22.0	45.7	NA	−48.5	19.8	NA
$\Delta G^{\neq}_{323}$	29.8	40.6	NA	14.7	23.1	NA
	b) Periodic calculations (PBE0-D2) with slab model					
		Type I			Type II	
$\Delta E^{\neq}_0$	37.0	32.6	35.7	11.4	28.1	29.1
$\Delta G^{\neq}_{323}$	101.9	32.8	90.6	65.8	28.0	87.0
	c) Extended cluster calculation (PBE0/6-311 + g(d,p)-D3)					
$\Delta E^{\neq}_0$	9.9	53.3	49.7	12.3	53.0	34.1
$\Delta G^{\neq}_{323}$	59.8	50.5	114.9	67.5	54.2	89.1
	d) Extended cluster calculation (B3LYP/6-311 + g(d,p)-D3)					
$\Delta E^{\neq}_0$	−9.2	34.2	33.5	3.5	38.5	22.8
$\Delta G^{\neq}_{323}$	40.7	31.4	98.6	58.7	39.7	77.8
	e) Homogeneous catalytic conversion with species **7** = VO(L)-(OO*t*Bu) and species **8** = VO(L)(OH)(OO*t*Bu): B3LYP/6-311 + g(3df,2p)-D3[a]					
		L = acac			L = OAc	
$\Delta E^{\neq}_0$	14.6	38.5	48.8	8.9	38.4	22.2
$\Delta G^{\neq}_{323}$	68.4	38.8	108.7	61.4	33.5	80.9

[a] Results from Ref. [21]. NA: not applicable owing to steric limitations. Note that the level of theory for optimization is not the same as the one applied for the displayed energy refinements. See computational methods for details.

the higher barriers predicted in the other models. Similar features are observed at a vanadium center of type A. This finding can be ascribed to a somewhat constrained confinement effect, as a result of the limited space around the active vanadium center, and may be regarded as unrealistic with the cyclohexene molecule described in the gas phase. More specifically, there is a strong stabilizing hydrogen bond between an underlying OH group and the alkylperoxo group in the transition state. At the active site B in the interior of the material, the epoxidation reaction from an active V^{+V} complex (e.g., **12**→**11**) can even not take place owing to space limitations. On the other hand, the radical decomposition reaction **7**→**9** does not suffer from space limitation and needs a free-energy barrier of 23.1 kJ mol^{-1}. In conclusion, reaction sites of the kind encountered in interior defect models of type A and B are too confined in space to be realistic. The cavity in the interior can further be enlarged by continuing the leaching process following the protocol leading to the construction of active sites of the type illustrated by the last two unit cells displayed in Figure 2. Such a description needs an enlargement of the supercell, and is scarcely feasible on the computational level. For further assessment, the periodic slab model will be used.

Extended cluster model: reactivity of cyclohexene oxidation

The various defect structures constructed in the periodic models discussed above enable the construction of extended clusters as shown in Figure 3. In the following we will assess how far such models describe the correct reactivity for cyclohexene oxidation pathways, compared with the periodic calculation. This information is interesting as the construction of reaction pathways with extended cluster models is far less demanding than with periodic calculations. In the latter, localization of transition states is not straightforward and the determination of normal modes is computationally very demanding. As the defect structures of type A and B are too limited in space, the predicted kinetics are too largely affected by the space confinement. It is unrealistic to expect that their results can be reproduced by cluster predictions. Therefore, we regard the reaction kinetics simulated in the periodic slab as the reference data for the cluster calculations. Results are also tabulated in Table 1. Cluster predictions using the same functional as in the periodic PBE0-D2 calculations are better suited to be submitted to a comparative study. The most significant deviations are observed in the barrier of the radical decomposition reaction **7**→**9** switching the oxidation state for vanadium from +IV to +V. Periodic calculations predict barriers of circa 30 kJ mol^{-1}, independent of the structure of the active site, but clearly much smaller than the 54 kJ mol^{-1} predicted in the cluster model using the same density functional (see Table 1 b and c). This is remarkable as the epoxidation barriers do not vary much. To elucidate this, we display the transition-state structures for both active sites in the periodic slab in Figure 4 (transition-state structures in the extended cluster model are taken up in Figure S3), from which essential features can be extracted. The epoxidation reaction described in this study follows a Sharpless-type mechanism. In this scheme the distance between the cyclohexene and the oxygen of the peroxo ligand of the complex plays a prominent role. In the transition state **12**→**11** this distance is the shortest (≈2.20 Å) and the O–O distance in the peroxo ligand also turns out to be the largest. These distances are ideal to promote the Sharpless mechanism as the main reaction mechanism for the cyclohexene epoxidation. They are regarded as reference values for the transition-state structures resulting from cluster calculations. These distances, reported in Figure S3, do indeed agree fairly well with the periodic predictions. As a result, the free-energy barriers for the **12**→**11** epoxidation reaction are also very close to each other (87 versus 89 kJ mol^{-1}) in the case of a reaction site of type II. The cluster predictions obtained with another level of theory (B3LYP/6-311 + g(d,p)-D3) are in line with previous results.[21]

To elucidate the discrepancy observed in the barrier of the radical decomposition reaction **7**→**9** in periodic versus cluster predictions, we notice a significantly larger value for the breaking O–O distance in the cluster model (1.80 versus 1.63–1.65 Å; Figures S3 and S4). This could probably be ascribed to the different functional used for optimization (PBE versus B3LYP) and to the different environment employed in both approaches. However, consistent use of the same DFT method (B3LYP/6-311 + g(d,p)-D3) in the extended cluster model for geometry optimization and energy calculation yields free-energy barriers of 31.4 and 39.7 kJ mol^{-1} for the radical reaction **7**→**9** at the two types I and II of active sites. These numbers are now much

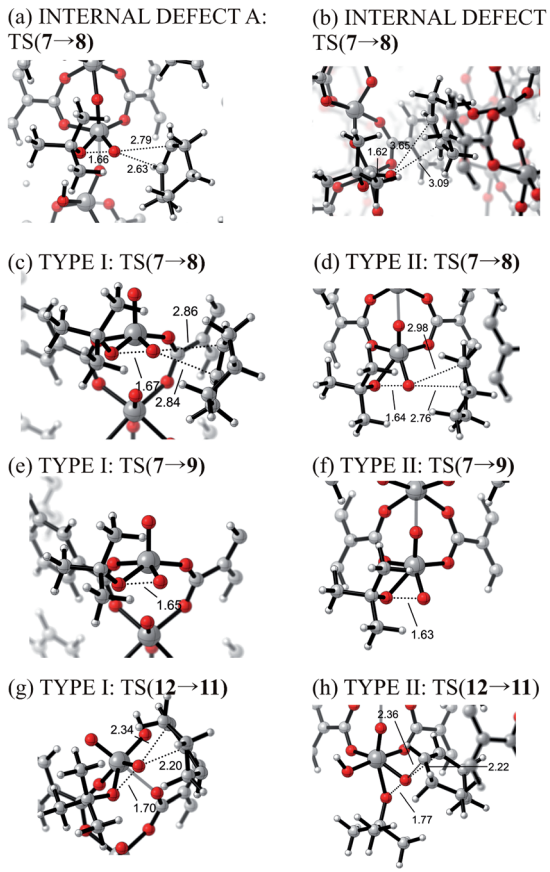

Figure 4. Transition-state (TS) structures in the periodic calculations. a, b) Defects of type A and B as displayed in Figure 2. c–h) Defects of type I and II in the slab model as displayed in Figure 3. Relevant distances are given in Ångstrom.

more in agreement with the periodic predictions of 32.8 and 28.0 kJ mol^{-1}.

The new theoretical data confirm what has been reported before.[20] There are two competitive cyclohexene epoxidation pathways: the first starting from an active $V^{+IV}O(OOtBu)$ complex (**7**→**8**) and the second through an active $V^{+V}O(OOtBu)$ complex (**12**→**11**). The first complex prefers kinetically to follow a radical generation reaction **7**→**9** switching the oxidation state for vanadium from +IV to +V. A V^{+V}–V^{+IV} recycling step **12**→**6** is not excluded, but this step is energetically less favored. Although all pathways are very competitive, we expect the epoxidation route via the $V^{+V}O(OOtBu)$ species **12** to be dominant because of the higher number of active V^{+V} species,[20] and decided to consider the **12**→**11** epoxidation reaction as the model reaction in the further investigation of the effect of linker substitution.

It is also instructive to discuss the similarities found in the cyclohexene epoxidation for the homogeneous catalytic system $VO(acac)_2$ with TBHP as oxidant. In a recent paper[21] the authors performed an extensive theoretical study involving all possible reaction paths leading to the epoxidation mechanism, taking into account various ligand-exchange reactions taking place among the active and inactive complexes in which vanadium may either have oxidation state +IV or +V. Radical decomposition reactions transforming V^{+IV} to V^{+V} species and vice versa have also been taken into consideration in the extended model space of active and inactive complexes with ligands varying from hydroxyl (OH) to acetylacetonate (acac), acetate (OAc), or *tert*-butoxide anion (O*t*Bu). A comparison between both studies is instructive as the similarities are large: only the ligand L differs substantially. In the current study the ligand is bidentate and contains two terephthalate linkers, which simulates the topology in some way, whereas in reference [21] the ligand is essentially less bulky. We can assume that the acac and OAc ligands are best comparable with the TA ligand in the current study. The energy barriers of these two selected active species are also reported in Table 1. The barriers agree to a large extent with those predicted in the heterogeneous catalyst. With the acetate ligand the agreement is even more striking. These results confirm our earlier hypothesis that the homogeneous catalytic system $VO(acac)_2$ is a good model system for the heterogeneous MIL-47 catalyst. This was also observed in reference [19] from an experimental point of view.

Summarizing, the proposed extended cluster of type II fits the requirements we imposed on the cluster model to mimic at best the periodic results. In addition, type II sites are thermodynamically more stable than type I sites. In the remainder of this article we will further elaborate on this cluster model.

Experimental results on the MIL-47-X series

To investigate the influence of substituents on the catalytic performance, a set of catalytic experiments was performed on the parent MIL-47 and MIL-47-X series (X = OH, Br, Cl, F, CH_3, NH_2). The time-conversion plot for the formation of cyclohexene oxide in the first catalytic runs is shown in Figure 5 whereas the values of turnover number (TON), turnover frequency (TOF), and vanadium leaching for the catalysts are presented in Table 2. Owing to the high amounts of vanadium leaching obtained after 6 hours of catalysis for all the compounds except MIL-47 and MIL-47-NH_2, only the first hour of the catalytic process can be assumed to be mainly heterogeneous. During this period, the TOF values follow a trend: MIL-47-OH > MIL-47-Br > MIL-47-Cl > MIL-47-F > MIL-47-CH_3 > MIL-47-NH_2 > MIL-47 (Table 2). Thus, all the substituted MIL-47-X catalysts show higher activity towards the formation of cyclohexene oxide relative to the parent MIL-47, thus indicating a significant effect of the functionalization on the catalytic performance.

We tried to correlate this trend of catalytic activity with the electronic effect of the grafted functional groups. In essence, a Hammett-type structure–activity linear free-energy relationship (LFER) can be established using the experimental rate constants (k_X) and Hammett's σ (substituent constant)[25] values of the substituents. The plot of $\log(k_X/k_H)$ versus σ should result in a Hammett–Taft equation[26] of the type: $\log(k_X/k_H) = \rho\sigma + E_s$, in which ρ and E_s represent the reaction constant and steric substituent constant, respectively.

As the substituents can never reside in a *para* position to a carboxyl group in the case of terephthalate substitution, we are limited in examining the LFER only as a function of the

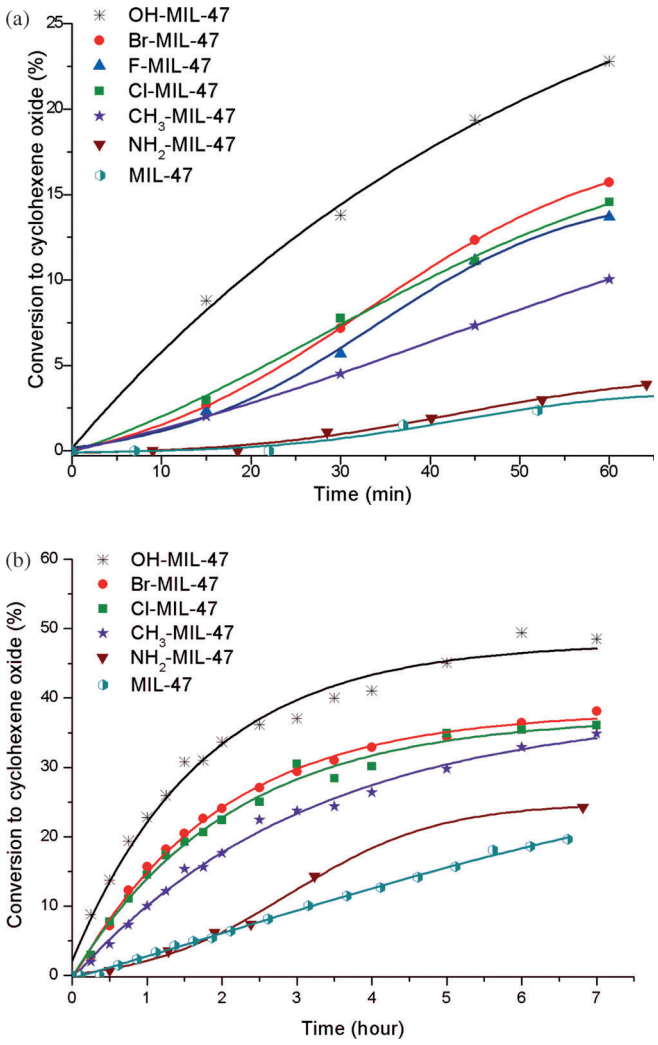

Figure 5. a,b) Catalytic conversion of cyclohexene to cyclohexene oxide for MIL-47 in comparison with substituted MIL-47. TBHP in decane as oxidant was used with chloroform as solvent.

Table 2. TOF, TON, and the percentage of leached V for the consecutive catalytic runs with TBHP/decane as oxidant.

Catalyst	TON_{ox}[a]	TOF_{ox} [h^{-1}][b]	Leaching [%][c]	V [mmol]
MIL-47 1st run[d]	17.8	2.6	< 3	0.46
MIL-47 2nd run	8.3	1.4	0.0	0.33
MIL-47-NH_2 1st run	29.7	4.4	10.2	0.38
MIL-47-NH_2 2nd run	53.7	9.0	8.8	0.13
MIL-47-OH 1st run	43.1	27.2	< 15	0.42
MIL-47-F 1st run	–	13.1	> 30	0.43
MIL-47-Cl 1st run	36.3	14.8	> 30	0.42
MIL-47-Br 1st run	41.3	17.3	> 30	0.42
MIL-47-CH_3 1st run	33.7	9.5	> 30	0.41

[a] TON_{ox} values were calculated after 6 h. [b] TOF_{ox} values were calculated after 30 min. All the TON_{ox} and TOF_{ox} values were calculated based on the conversion to cyclohexene oxide. [c] The amount of vanadium leaching was determined after 6 h. [d] Ref. [21].

meta substituent constant σ_m. A Hammett plot is displayed in Figure 6. The linear fit through the points belonging to monoatomic substituents goes through the origin of the plot, and

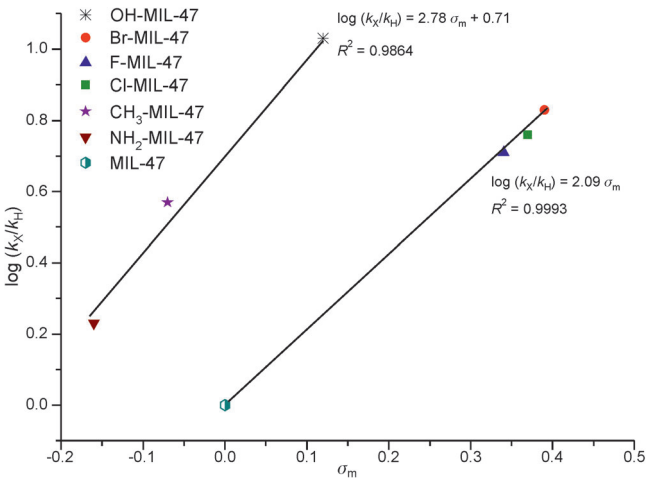

Figure 6. Hammett plots for the cyclohexene epoxidation on different MIL-47-X catalysts as a function of the substituent value σ for substituents at the *meta* position of the active site.

gives evidence that no steric effects are playing a role ($E_s = 0$). On the contrary, in the case of multiatomic substituents, such as OH, NH_2, and CH_3, a steric substituent coefficient of $E_s = 0.71$ is observed. The OH substituent constant σ_m(OH) is determined by deprotonation of a carboxylic acid with OH in the *meta* position, which indicates that there is no extra hydrogen bond with the carboxyl group connected to the active site. This explains why the OH group follows nicely the trend of the multiatomic substituents. In a realistic situation we can, however, have OH groups both in either a *meta* or *ortho* position—or even more likely in a *meta–ortho* combination—relative to the carboxyl group connected to the active site. One of the computational tasks will be to carefully address some possible substituent orientations.

Recently, the UiO-66-X series was tested for the cyclization of citronellal. It was found that the defect linkers were responsible for the catalytic activity. For the UiO-66-X series, a Hammett equation as a function of σ_m[17] could also be found, in which electron-withdrawing substituents led to an increased rate and electron-donating substituents to a decreased rate. The electronic modulation effect on the conversion was in the same line as in the case of the epoxidation with MIL-47-X: a reaction constant $\rho = 2.35$ was found compared with 2.09 in the latter case. Furthermore, the Hammett–Taft equation did not lead to any steric substituent effect ($E_s = 0$). Those results were not surprising, since the substituents in a *meta* position with respect to the carboxyl group connected to the active Zr site cannot have much steric influence on the transition state.

After longer periods some catalysts become more active but this may be ascribed to the formation of more defects in the material and larger amounts of leached vanadium centers. At this point, homogeneous pathways may also contribute to the higher activity. Although MIL-47-NH_2 showed much less leaching than the other substituted MIL-47-X after 6 hours of conversion, this did not lead to a decreased initial activity for MIL-47-NH_2. The initial number of active sites in the MIL-47-X materials should thus be similar. From an experimental point of

view it is hard to differentiate between reactions taking place on heterogeneously active sites or on homogeneously working active sites owing to leaching. To illustrate the difference in catalytic activity of both active sites, the epoxidation reaction of cyclohexene has also been performed in a reaction mixture of vanadyl acetylacetonate $VO(acac)_2$ and OH-functionalized terephthalate linkers, thereby creating in this way some "homogeneous" variant of the heterogeneous MIL-47-OH catalyst. By respecting equal amounts of vanadium species and linkers, we create a mixture that proportionally resembles the reaction solution that is found after leaching of fractions of the crystalline material. We may expect that their catalytic activity will behave in a similar way. The conversion plots are shown in Figure S5 and S6, and they reveal that the homogeneous vanadium centers do indeed act as a very efficient homogeneous catalyst, which leads to a higher conversion of cyclohexene, especially during the initial stages of the reaction. Figure S6 shows that after 5 hours the homogeneous and heterogeneous plots coincide with each other. The conversion plots are very clear: the formation of the epoxide product is much faster for the homogeneous variant and the convergence pattern is reached after 1.5 hours, thus indicating that there are more active V species in the homogeneous catalyst relative to the MIL-47-OH.

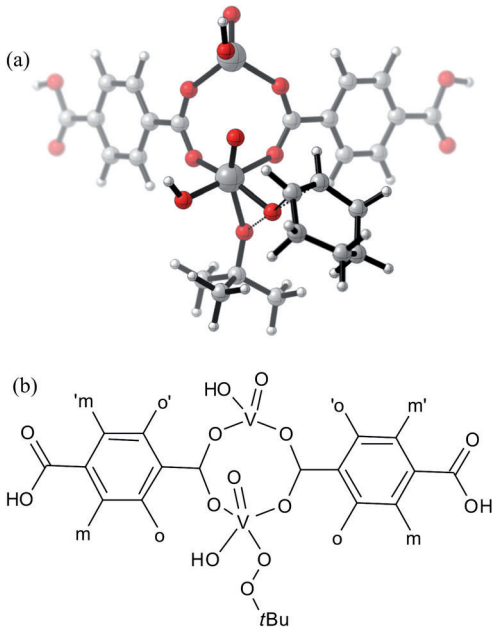

Figure 7. a) Investigated epoxidation transition state on the unsubstituted MIL-47 cluster. b) The MIL-47-X cluster models consider four substitution positions: *ortho* (o), *meta* (m), *ortho'* (o'), and *meta'* (m'). For example, the notation *meta/ortho* stands for a substituent on the left linker in the *meta* position and a substituent on the right linker in the *ortho* position. By convention the right linker is closest to the alkylperoxo group.

Theoretical results on the MIL-47-X series

Based on the conclusions drawn above with regard to the structure of the active site and the rate-determining step in the cyclohexene oxidation with TBHP in MIL-47, we investigated the effect of linker substitutions on the epoxidation rate of $V^{+V}O(OOtBu)(OH)$ species **12** on an active site of type II. The basic cluster upon which substitutions can be performed is displayed in Figure 7a, in which the transition state is visualized for the **12**→**11** epoxidation reaction.

In principle the substituents may be placed at various positions as indicated in Figure 7b. If we assume that each organic linker is functionalized there are in total 16 distinct combinations. Each combination corresponds with a distinct cluster, which can be defined by the notation X-$_{i/j}$ in which *i* and *j* refer to the position of the substituent X on the left/right linker. By convention the right linker is closest to the alkylperoxo group. Not all positions are equally interesting; one can expect that the global electronic modulation of the functionalized linkers is larger for *ortho*/*meta* positions than for *ortho'*/*meta'* positions, with the convention that *ortho'*/*meta'* is further away from the active V center (see Figure 7b). Owing to the high computational cost in considering all possible pairs *i*/*j*, we limit our selection to *ortho*/*ortho*, *meta*/*meta*, *ortho*/*meta*, *meta*/*ortho*, *ortho'*/*meta'*, and *meta'*/*ortho'*. The last two combinations have been added to verify if its electronic modulation has indeed a negligible effect on the rate constant for epoxidation, as intuitively expected. As averaging procedure we introduce a Boltzmann weight factor $\exp\left\{-\frac{\Delta G^0_{i/j}}{k_B T}\right\}$ for each variant *i*/*j* of active site with $\Delta G^0_{i/j}$ the Gibbs free energy of formation relative to the most stable isomer of the MIL-47-X series. The average rate constant, which could be associated with the ensemble of active sites in MIL-47-X and which in principle should match at best the experimentally measured value, is then elaborated as [Eq. (1)]:

$$< k_X >_{stat} = \frac{\sum_{i/j} \exp\left\{-\frac{\Delta G^0_{i/j}}{k_B T}\right\} k_{i/j}}{\sum_{i/j} \exp\left\{-\frac{\Delta G^0_{i/j}}{k_B T}\right\}} \quad (1)$$

For each structural isomer, characterized by the pairwise indices *i*/*j*, of the MIL-47-X series with functional group X = OH, F, Cl, or NH_2, the geometry of the cluster representing the active $LV^{+V}O(OOtBu)(OH)$ site has been optimized in an unconstrained fashion, that is, all atoms were allowed to relax. In a previous paper on the parent MIL-47 material, we have shown that a description of the reaction in the unconstrained or constrained cluster model leads to similar kinetic and thermodynamic results.[21] Owing to the existence of many transition states, it is not always trivial to deduce the correct state for the reactants, that is, $LV^{+V}O(OOtBu)(OH)$ and the cyclohexene molecule in the gas phase. We therefore applied consistently the following procedure. First, the structure of the desired transition state was determined. In the second step the cyclohexene molecule was removed and the remaining structure reoptimized. Depending on the specific position of the functional group substituted on the linker, the energies of formation will vary among the different clusters under consideration. Table 3 reports the relative free energies between the various active $LV^{+V}O(OOtBu)(OH)$ metal sites in each MIL-47-X

Table 3. Differences in free energy of formation [kJ mol^{-1}] between the various active LV^{+V}O(OO*t*Bu)(OH) sites at 323 K with varying position of the functional group on the linker. Forward rate constants for the epoxidation reaction **12**→**11** in units of m^3 mol^{-1} s^{-1} (apparent kinetics). Ratios with respect to the parent MIL-47 (X = H) are also given per individual reaction (weighted). The Boltzmann statistical ratio $<k_X>_{stat}/k_H$ is calculated according to Equation (1).

X	ΔG^0 [kJmol^{-1}]	k_X	k_X/k_H	$<k_X>/k_H$ (weighted)
H	0.00	1.24×10^{-3}	1.00	1.00
NH_2				–
ortho/ortho	1.83	1.35×10^{-2}	10.81	–
meta/meta	7.93	2.92×10^{-3}	2.35	–
ortho/meta	0.00	1.00×10^{-4}	0.08	–
meta/ortho	3.60	4.95×10^{-2}	39.81	–
ortho′/meta′	19.56	2.00×10^{-3}	1.61	–
meta′/ortho′	14.99	3.89×10^{-4}	0.31	–
theory (stat)	–	–	–	8.81
exptl	–	–	–	1.7
F				
ortho/ortho	3.30	5.85×10^{-3}	4.70	–
meta/meta	3.32	5.51×10^{-3}	4.43	–
ortho/meta	0.00	2.21×10^{-3}	1.78	–
meta/ortho	3.77	3.14×10^{-3}	2.53	–
ortho′/meta′	1.75	2.81×10^{-3}	2.26	–
meta′/ortho′	0.14	3.23×10^{-3}	2.59	–
theory (stat)	–	–	–	2.64
exptl	–	–	–	5.0
Cl				
ortho/ortho	0.96	3.73×10^{-3}	3.00	–
meta/meta	3.02	2.70×10^{-3}	2.17	–
ortho/meta	0.00	3.18×10^{-3}	2.56	–
meta/ortho	2.09	5.68×10^{-3}	4.57	–
ortho′/meta′	3.95	3.70×10^{-3}	2.98	–
meta′/ortho′	2.21	3.88×10^{-3}	3.12	–
theory (stat)	–	–	–	3.02
exptl	–	–	–	5.70
OH				
ortho/ortho	2.16	3.28×10^{-1}	263.95	–
meta/meta	5.82	5.78×10^{-4}	0.46	–
ortho/meta	0.00	2.40×10^{-4}	0.19	–
meta/ortho	0.85	1.09×10^{-1}	87.89	–
ortho′/meta′	23.50	1.72×10^{-3}	1.39	–
meta′/ortho′	22.90	2.31×10^{-3}	1.86	–
theory (stat)	–	–	–	79.59
exptl	–	–	–	10.5

series. Note that the free-energy differences are enthalpy driven (Table S6).

In all cases the position *ortho*/*meta* is energetically preferred, and is more stable than the configuration with the two substituents both in the *ortho* position. Many features lie on the basis of this finding. A first aspect is the position of the substituent with regard to the vanadium of the active site (see Figure 7b), which determines to a large extent the electrostatic interaction between the two atoms. The second aspect is the presence of hydrogen bonds, which can be formed depending on the spatial orientation of the multiatomic substituent (in the case of OH and NH_2) and which stabilize the conformation. Resonance effects take place in the molecular system not only in the phenyl ring of the terephthalate linker, but also in rings that are occasionally constructed by the presence of the hydrogen bonds. It is a complex interplay of all these features that ultimately determines the final electronic modulation induced by the substituent. Not surprisingly, it can vary strongly per case.

In an attempt to elucidate the different electronic modulation patterns induced by the substituents, we investigated the charge shift occurring in the linkers as a result of the functionalization of the linkers. Several charge population schemes can be used (Mulliken, Becke,[27] Iterative Stockholder,[28] Hirshfeld,[29] Hirshfeld-i,[30] Hirshfeld-e[31] partitioning). One of the most recent partition schemes is offered by Hirshfeld-e combining electrostatic potential accuracy with transferability.[31] Their charge predictions for the TA linkers (including the two carboxylate oxygen atoms; Figure 7) and for the benzoic linkers (excluding the two carboxylate oxygen atoms) are given in Table 4. We only take up the results for the energetically most

Table 4. Extended Hirshfeld charges of the LV^{+V}O(OO*t*Bu)(OH) clusters of MIL-47-X with X = NH_2, F, Cl, and OH. The charge on different parts of the system is given. The atoms included in TA linkers and Benzoic linkers are shown in Figure S.9.

		Pre-TS			TS	
X	V	TA linkers	Benzoic linkers	V	TA linkers	Benzoic linkers
H	–	1.11	−0.64	−0.07	0.97	−0.63	−0.10
NH_2	*m/o*	1.11	−0.63	−0.08	0.97	−0.61	−0.09
F	*o/o*	1.08	−0.63	−0.10	0.96	−0.62	−0.12
Cl	*m/o*	1.10	−0.65	−0.09	0.97	0.63	−0.10
OH	*o/o*	1.10	−0.69	−0.15	0.98	−0.68	−0.18

favorable positions of the substituents. Different positions may cause some slight variations of the charges on the linkers, but the main trend is given by the type of substituent rather than its position (the whole list is given in the Supporting Information). With respect to the parent MIL-47, which we regard as the reference, the linkers with electron-withdrawing substituents attract more electronic charge than NH_2. The hydroxyl group is the most electronegative by far, enforced by the formation of electric dipoles that are formed in the various hydrogen bonds present in MIL-47-OH (see Figure 8b). Results derived from other charge population schemes are taken up in the Supporting Information.

During the reaction there is some slight electronic charge transfer from the catalytic site to the benzoic linkers (also in the case of the parent MIL-47). Even the (positive) charge of the active vanadium center is submitted to some charge drop. In the transition state, electronic charge is transferred from the alkylperoxo complex to the catalyst. The more electron density is present on the benzoic linker, the higher the reaction rate for the epoxidation reaction. The total charge for the benzoic linkers in the parent catalyst amounts to −0.07 and becomes more negative for all substituents considered in this study. All substituted MIL-47-X catalysts show higher activity both experimentally and theoretically towards epoxidation than the

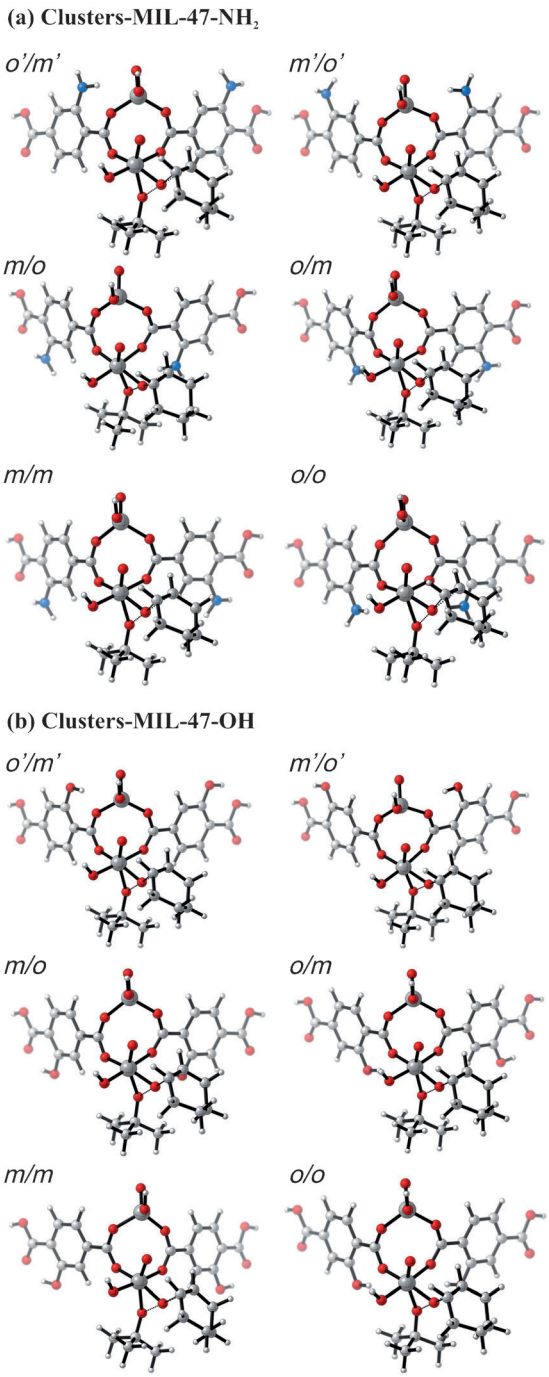

Figure 8. The optimized transition states for amino- and hydroxo-substituted MIL-47 clusters in the epoxidation reaction with cyclohexene. Relevant hydrogen bonds stabilizing the transition state are indicated. Distances in Ångstroms. Notation m/o, o/m, o/o, and m/m follows the convention of Figure 7.

parent MIL-47, so there is a clear correlation between the charge concentrated on the linker and the reaction rate constant.

The transition states for the epoxidation reaction **12**→**11** in the parent MIL-47 cluster and some of the substituted clusters are shown in Figures 7a and 8. The *tert*-butoxy group is coordinated with one vanadium center whereas the cyclohexene is located in a free spot in front of the two linkers. This particular transition state, which involves quite bulky groups from all reactants, stresses once more that structural defects need to be introduced into the periodic structure to allow enough space for the reaction to take place. In the case of the hydroxo clusters (Figure 8), the hydrogen atoms of the OH groups provide extra stabilization for the transition state through hydrogen bonds, which are formed in the epoxidation transition states. The obtained kinetic data are collected in Table 5, together with the enthalpy and entropy contributions to the Gibbs free-energy barriers. All energies are referred to the separated reactants and thus "apparent" reaction kinetics are obtained.

We notice some significant differences in the free-energy barriers depending on the particular substituent position. They are all energetically driven; the entropic contributions are fluctuating around the value of 58.7 kJ mol^{-1} corresponding with the unsubstituted species and are not decisive in causing an increase of the catalytic activity. Some substituent positions are manifestly more favorable than others generating a decrease of the free-energy barrier of more than 10 kJ mol^{-1}. They all prefer the substituent in an *ortho*/*ortho* or a *meta*/

Table 5. Kinetic data for the epoxidation reaction of a substituted $V^{+V}O$-(OO*t*Bu) cluster representing MIL-47-X (X = NH_2, Cl, and OH) with cyclohexene at 323 K. Free-energy barriers ($\Delta G^{\neq}$), enthalpy ($\Delta H^{\neq}$), and entropy contributions ($-T\Delta S^{\neq}$) are given in kJ mol^{-1}. The forward rate constants k are given in units of m^3 mol^{-1} s^{-1} (apparent kinetics).

X	$\Delta G^{\neq}$ [kJ mol^{-1}]	$\Delta H^{\neq}$ [kJ mol^{-1}]	$-T\Delta S^{\neq}$ [kJ mol^{-1}]	k_X [m^3 mol^{-1} s^{-1}]
H	87.5	28.9	58.7	1.24×10^{-3}
NH_2				
ortho/ortho	81.1	19.5	61.6	1.35×10^{-2}
meta/meta	85.3	27.3	57.9	2.92×10^{-3}
ortho/meta	94.3	36.5	57.8	1.00×10^{-4}
meta/ortho	77.6	18.4	59.2	4.95×10^{-2}
ortho′/meta′	86.3	27.6	58.7	2.00×10^{-3}
meta′/ortho′	90.7	30.5	60.2	3.89×10^{-4}
F				
ortho/ortho	83.4	26.6	56.8	5.85×10^{-3}
meta/meta	83.5	27.2	56.3	5.51×10^{-3}
ortho/meta	86.0	28.9	57.1	2.21×10^{-3}
meta/ortho	85.1	27.5	57.6	3.14×10^{-3}
ortho′/meta′	85.3	27.9	57.4	2.81×10^{-3}
meta′/ortho′	85.0	28.9	56.1	3.23×10^{-3}
Cl				
ortho/ortho	84.6	22.5	62.1	3.73×10^{-3}
meta/meta	85.5	28.9	56.5	2.70×10^{-3}
ortho/meta	85.0	28.0	57.0	3.18×10^{-3}
meta/ortho	83.5	23.5	60.0	5.68×10^{-3}
ortho′/meta′	84.6	26.9	57.7	3.70×10^{-3}
meta′/ortho′	84.5	28.3	56.2	3.88×10^{-3}
OH				
ortho/ortho	72.6	18.7	53.9	3.28×10^{-1}
meta/meta	89.6	31.3	58.3	5.78×10^{-4}
ortho/meta	92.8	29.9	62.1	2.40×10^{-4}
meta/ortho	75.5	20.7	54.8	1.09×10^{-1}
ortho′/meta′	86.7	26.6	60.1	1.72×10^{-3}
meta′/ortho′	85.9	27.1	58.8	2.31×10^{-3}

ortho position. The catalytic performance of these functionalized materials is largely determined by those configurations with substituents on preferential positions. They determine to a large extent the weighted average $<k_X/k_H>_{stat}$ and lie at the origin of the significant enhancement of the epoxidation rate constant as reported in Table 3. The overall agreement with the experimental TOF_X/TOF_H ratios is quite satisfactory (last column in Table 3). The largest enhancement is noticed for MIL-47-OH. Theory overestimates the enhancement and this is mainly owing to the two dominant contributions arising from the *ortho*/*ortho* and *ortho*/*meta* conformations. Probably the orientation of the electron-withdrawing hydroxyl group in our cluster model lies on the origin of a strong hydrogen bond attracting too much electron density from the carboxyl group. This is illustrated in the bottom-left structure of Figure 8 displaying the transition state with the OH group in the *ortho* position. There are also other features that require attention: the apparent difference by three orders of magnitude in the prediction of the epoxidation rate constant between the hydroxyl substituent in the *meta*/*meta* and *ortho*/*meta* position on the one hand and in the *ortho*/*ortho* and *meta*/*ortho* position on the other hand. The mean reaction rate is determined completely by one or two conformations with substituents on preferential positions. We will briefly elaborate on the explanation for the mismatch in rates by analyzing the charges of the linkers for some preferential positions of the functional groups (Table 4). We refer to the Supporting Information for a more complete overview of the charge distributions in the prereactive complex and transition state. The charge of the V center does not change on functionalizing the linker with a substituent. The presence of a functional group results in a charge transfer from the alkylperoxo complex to the linkers, and this feature appears to have a significant influence on the epoxidation rate constant.

The appearance or disappearance of hydrogen bonds in the transition state compared with the prereactive complex may affect the reaction barrier to a large extent. The transition state in the *ortho*/*ortho* conformation of MIL-47-OH is clearly stabilized by the H bond between the hydrogen of the OH substituent in the *ortho* position and one of the peroxo oxygen atoms (bottom-left structure in Figure 8), whereas in the *meta* position this H bond does not occur (bottom-right structure in Figure 8). The situation is even more dramatic in the case of NH_2 as substituent. In the prereactive complex with an amino hydrogen in the *ortho* position with respect to the vanadium alkylperoxo group, a strong hydrogen bond is formed with the oxygen of the hydroxyl group bound with the metal. This bond disappears completely in the transition state inducing a serious increase of the free-energy barrier by more than 16 kJ mol^{-1} compared with the *meta*/*ortho* conformer. This lies at the origin of the fact that these MIL-47-NH_2 species are significantly better stabilized than the other amino-functionalized MIL-47 variants. Combined with a larger epoxidation rate constant these two species (*ortho*/*ortho* and *meta*/*ortho*) determine the average enhancement with respect to the reference (unsubstituted active site), and this largely explains the observed overestimation with respect to experiment (8.8 versus 1.7). Similarly for MIL-47-OH, we have an overestimation with respect to experiment (79.6 versus 10.5). These features are inherent to the usage of a static approach, in which the energetically most stable geometrical configuration is that with the strongest hydrogen bonds. In reality the orientation of the amino group fluctuates and can best be reproduced in molecular dynamics simulations. In such a model, we expect that the weighted $<k_X>/k_H$ factor will decrease, and might come closer to the experimental value.

In the case of a halogen-functionalized MIL-47 variant, the issue of a preferential spatial orientation of the substituent is completely missing. No hydrogen bonds are formed, and all conformations show more or less the same stability and catalytic activity, independent of the position of the substituent (F or Cl). Theory predicts an enhancement by a factor of 2.6, close to the experimental value of 5.0.

Summarizing for a multiatomic substituent, the variations in catalytic activity can largely be affected by the substituent position. The slightly overestimated theoretical enhancement noticed at the catalyst MIL-47-NH_2 is largely a result of the strong hydrogen bonding of the amino hydrogen atoms with the carboxylate oxygen atoms. As experiment is unable to disentangle the different positions, the theoretically observed optimal positions for the substituents cannot be verified. The experimentally measured enhancement in the cyclohexene epoxidation performance is a statistical average. In all cases the presence of substituents on the linkers does increase the epoxidation rate constant, and this trend is in line with theory.

Conclusion

In this study, we have tested both experimentally and theoretically the effect of linker modifications on the metal–organic framework MIL-47—containing coordinatively saturated V^{+IV} sites linked by terephthalate linkers—for the epoxidation of cyclohexene. The use of periodic models is indispensable to take the environment of the active site fully into account, but the high computational cost and the intensive efforts needed to perform correct frequency analyses make it a tool for occasional assessment rather than for routine kinetic studies. On the other hand, extended cluster models require a substantially lower computational cost and are better suited to locate transition states and to determine the normal modes, which are indispensable for a proper computation of the entropy contributions. The effect of linker substitution was therefore investigated on a cluster model. The size and structure of the extended cluster are determined on the basis of a comparison of the kinetics predicted by the periodic model and the cluster model. We do indeed find that all substituents, such as F, Cl, Br, CH_3, and NH_2, give higher rates of epoxidation as was observed experimentally. The largest increase was found for the OH substituent, in agreement with experiment. Theoretically various positions of the substituents are possible and we calculated relative rates compared with the unmodified material based on a statistical method that incorporates the relative probabilities of the various clusters. The governing factors for the increase may be ascribed to specific interactions in the transition

state, such as a hydrogen bond between an electron-donating or -withdrawing functional group in the *ortho* position with a neighboring carboxylate group connected to the vanadium atom. They generate charge transfers to the linkers. Overall, a good qualitative agreement is found between the electronic modulation of a selection of substituents (OH, F, Cl, NH_2) and the experimentally observed catalytic activity for MIL-47-type materials for cyclohexene oxidation. From an experimental point of view, we can conclude that the substituted MIL-47 materials are much more prone to leaching during the epoxidation catalysis than the parent MIL-47, which makes them less interesting for industrial applications, in which the stability of the materials is mandatory. Yet, with the recent development of mixed-metal MOFs with vanadium (e.g. V, Fe), one can expect that the stability of these V-MIL-47 frameworks can still be increased with metal doping, which makes this study a valuable intermediate report towards more stable heterogeneous epoxidation catalysts.

Experimental Section

Computational methods

Periodic calculations

Periodic DFT calculations were performed with the help of the Vienna Ab Initio Simulation Package (VASP).[32] For all periodic simulations, the Brillouin zone sampling was restricted to the Γ point. Furthermore, the PBE exchange-correlation functional of Perdew, Burke, and Ernzerhof was applied[33] for optimization together with van der Waals corrections of type D2[34] as implemented in VASP 5.2.12. The projector-augmented wave (PAW) approximation[35] together with a plane-wave basis set (kinetic energy cutoff of 600 eV) was used. The RMM-DIIS algorithm was chosen as optimizer to converge the atomic forces below 0.01 eV $Å^{-1}$. A Gaussian smearing[32b] of 0.01 eV was also applied.

First, the cell vectors of MIL-47 were optimized starting from XRD data.[22] Second, the periodic slabs were constructed (see Results and Discussion and Figure 3), and the unit cell parameters were maintained throughout the whole computational study. The atoms within each periodic slab were allowed to move freely upon optimization of the slab. For the reaction pathways only the active site and the neighboring terephthalic groups were relaxed. During this partial optimization approach, the atomic forces were converged below 0.003 eV $Å^{-1}$.

Defects in the interior of the crystal were modeled with a slightly different procedure; all atoms were allowed to move freely applying a Gaussian smearing of 0.05 eV and self-consistent field (SCF) criterion of 10^{-6} eV while the forces were converged below 0.01 eV $Å^{-1}$.

Next, a partial vibrational analysis was performed including only the active site, which consisted of the central vanadium atom and nearest neighbors together with the reactive area (cyclohexene + *t*BuOO complexes). Displacements in the *a*, *b*, and *c* axes of ±0.015 Å were used in the subsequent partial Hessian calculation. The nature of the minima and transition states was very carefully checked and if residual imaginary frequencies were still present, the following strategies were used to get rid of them: 1) the convergence criterion for the electronic SCF problem was increased from 10^{-6} up to 10^{-10} eV;[36] and 2) a small displacement along the trajectory of the imaginary frequency was followed by a reoptimization of the found minimum. We refer to the Supporting Information for all structures subjected to the partial Hessian calculation.

All systems contained V^{+IV} atoms, which were modeled in their high-spin state fixing the value $N_\alpha - N_\beta$ to the number of V^{+IV} atoms in the unit cell. We anticipated that this had a negligible effect on the energy barriers of the material. The optimized geometries were used for single-point calculations at the PBE0-D2 level, employing a standard kinetic energy cutoff (400 eV) and SCF criterion (10^{-5} eV). For the dispersion part of the energy, D2 corrections according to Grimme were applied.[34,37]

Both PBE-D2 as PBE0-D2 results are taken up in the Supporting Information.

Extended cluster calculations on the various reactions within the catalytic cycle

Previously, a cluster model[21] had already been investigated by some of the present authors; it contained two active sites, of which only one was investigated. The constrained character of the MOF could be preserved by fixing the outer carboxyl oxygen atoms. For the optimization of the geometries, an ONIOM (our own *n*-layered integrated molecular orbital and molecular mechanics) approach was used to accurately describe the active site $(VO(COO))_2$ and the reacting molecules on a high level of theory and the surrounding linkers at a lower level of theory (Figure 2). Geometry optimizations were performed with the Gaussian 09 package[31] using the B3LYP hybrid functional.[38] Within the high-level part, the double-zeta Pople basis set 6-31 + G(d) was used for all high-level atoms for which the LANL2DZ effective core potential and basis set was applied.[39] For the sake of clarity, this combined basis will be abbreviated as BS1. Furthermore, the lower-level part was described at the B3LYP/3-21g level. The general optimization procedure could thus be abbreviated as ONIOM(B3LYP/BS1:B3LYP/3-21g). Afterwards, energy refinements, including the third version of dispersion corrections according to Grimme,[34] were executed at three different levels of theory (B3LYP/6-311 + g(d,p)-D3, PBE/6-311 + g(d,p)-D3, and PBE0/6-311 + g(d,p)-D3) to allow for a good comparison with the energies of the periodic simulations at the PBE-D2 and PBE0-D2 level of theory. Note that variations in the structures of the transition state obtained in the two calculations are marginal (compare Figures S3 and S4).

The procedure for the extended cluster calculations on the substituted MIL-47-X is similar. Only the application of an ONIOM approach was omitted to have a more reliable optimization of the substituent groups. Using the standard notation "LOT-E"//"LOT-G" (LOT-E and LOT-G are the electronic levels of theory used for the energy and structure optimizations, respectively), all results discussed herein were obtained with the method denoted as "B3LYP/6-311g(d,p)-D3//B3LYP/BS1". The calculation of all kinetic and thermodynamic parameters was performed using the in-house-developed software module TAMkin.[40]

In both cluster and periodic approaches, the partial Hessian vibrational analysis (PHVA) method,[41] as implemented in the in-house-developed post-processing toolkit TAMkin,[40] was then used to construct the partition functions, which were required to determine the kinetics of the studied reactions. The PHVA method was already applied successfully in previous first-principles studies on kinetics.[21,23,42] Use of PHVA is recommended in the constrained cluster calculations, as the outer carboxyl oxygen atoms have been fixed at their crystallographic position. In the case of the periodic

calculations, only a partial Hessian was constructed with finite differences to save computational time. The program ZEOBUILDER was used for the construction of initial geometries for the periodic calculations.[43]

Experimental procedures

Synthesis and activation of MIL-47-X materials

MIL-47 was synthesized according to a route described in the literature.[22] MIL-47-X compounds were prepared in a rapid microwave-assisted method as described below. The acronym "as" stands for as synthesized.

Synthesis of MIL-47-NH_2-as: A mixture of VCl_3 (267 mg, 1.74 mmol) and 2-aminoterephthalic acid (308 mg, 1.74 mmol) in water (3 mL) was placed in a Pyrex tube (10 mL). The tube was sealed and heated in a microwave synthesizer (CEM, Discover S) to 150 °C at 150 W, held under these conditions for 20 min with stirring, then cooled to room temperature. The greenish yellow precipitate was collected by filtration and dried in air.

Synthesis of MIL-47-F-as: A mixture of VCl_3 (100 mg, 0.64 mmol) and 2-fluoroterephthalic acid (117 mg, 0.64 mmol) in water (2 mL) was placed in a Pyrex tube (10 mL). The tube was sealed and heated in a microwave synthesizer (CEM, Discover S) to 170 °C at 150 W, held under these conditions for 30 min with stirring, then cooled to room temperature. The greenish yellow precipitate was collected by filtration and dried in air.

Synthesis of MIL-47-Cl-as: This compound was obtained as a greenish yellow powder by the procedure described for MIL-47-F, except the linker used was 2-chloroterephthalic acid (156 mg, 0.64 mmol) instead of 2-fluoroterephthalic acid.

Synthesis of MIL-47-Br-as: This compound was obtained as a greenish yellow powder by the procedure described for MIL-47-F, except the linker used was 2-bromoterephthalic acid (156 mg, 0.64 mmol) instead of 2-fluoroterephthalic acid.

Synthesis of MIL-47-CH_3-as: This compound was obtained as a greenish yellow powder by the procedure described for MIL-47-F, except the linker used was 2-methylterephthalic acid (115 mg, 0.64 mmol) instead of 2-fluoroterephthalic acid and the temperature used was 150 °C instead of 170 °C.

Synthesis of MIL-47-OH-as: This compound was obtained as a greenish yellow powder by the procedure described for MIL-47-F, except the linker used was 2-hydroxyterephthalic acid (116 mg, 0.64 mmol) instead of 2-fluoroterephthalic acid.

Activation of MIL-47-X-as: A suspension of each of MIL-47-NH_2-as and MIL-47-Cl-as in dimethylformamide was heated (125 °C, 1.5 h, MIL-47-NH_2-as; 150 °C, 5 h, MIL-47-Cl-as) in an oil bath. The solids were isolated by filtration and heated (80 °C, 2 h, MIL-47-NH_2-as; 320 °C, 24 h, MIL-47-Cl-as) under dynamic vacuum to give the activated forms of the compounds. A slow heating ramp (ca. 0.33 °C min^{-1}) to 80 °C, before being held at this temperature for 2 h, was crucial to activate the MIL-47-NH_2-as sample.

Each of MIL-47-Br-as, MIL-47-CH_3-as, and MIL-47-OH-as was heated directly (300, 300, and 280 °C, respectively) under dynamic vacuum for 24 h to obtain the evacuated forms of the compounds.

The MIL-47 sample, synthesized by using conventional electric heating, was calcined at 300 °C for 21.5 h in air to give the thermally activated compound.

Catalytic tests

During a typical catalytic test, a 100 mL round-bottom flask was charged with chloroform (30 mL, anhydrous) as solvent, cyclohexene (5 mL), and 1,2,4-trichlorobenzene (6.2 mL, used as internal standard for the GC analysis). The oxidant used was *tert*-butyl hydroperoxide (TBHP) dissolved as a 5.5 M solution in decane. The latter was chosen as oxidant because of the instability of MIL-47 in TBHP in water.[19] The molar ratio of cyclohexene/oxidant was 1:2. All the catalytic tests were performed at a temperature of 50 °C and with an Ar-containing balloon on top of the condenser. Blank reactions at this temperature showed no catalytic conversion of cyclohexene.

The reaction mixture was stirred under an argon atmosphere. Aliquots were gradually taken out of the mixture, diluted with ethyl acetate (500 μL), and subsequently analyzed by GC with flame ionization detection. After a catalytic run, the catalyst was recovered by filtration on a combined nylon-membrane filter, washed several times with acetone, and vacuum dried overnight. The filtrate was analyzed by X-ray fluorescence to determine the leached vanadium. To eliminate experimental noise and GC errors, a polynomial fit (of order 4) through the cyclohexene conversion was performed to determine the turnover frequency (TOF) and turnover number (TON), which were calculated after 30 min and 6 h of reaction time, respectively. In a similar fashion, the amount of cyclohexene oxide produced per catalytic site per hour was also calculated (TON_{ox}, h^{-1}) after 30 min to determine the average epoxidation rate per catalyst MIL-47.

Acknowledgements

M.V. acknowledges funding from both Scientific Research-Flanders (FWO) and the research board of Ghent University (BOF). V.V.S., P.V.D.V., and S.B. acknowledge funding obtained from Ghent University by the GOA grant no. 01G00710. K.L. acknowledges financial support from the BOF of Ghent University (postdoctoral grant). V.V.S. and M.W. acknowledge BELSPO in the frame of IAP-PAI P7/05. V.V.S. acknowledges funding from the European Research Council under the European Community's Seventh Framework Programme [FP7(2007–2013) ERC grant agreement number 240483]. Computational resources and services were provided by Ghent University (Stevin Supercomputer Infrastructure). Grants for computer time at the HLRN cluster of the North-German Supercomputing Alliance and the JUROPA cluster/FZ Julich are acknowledged.

Keywords: ab initio calculations · epoxidation · heterogeneous catalysis · metal–organic frameworks · substituent effects

[1] a) G. Férey, *Chem. Soc. Rev.* **2008**, *37*, 191 – 214; b) S. Kitagawa, R. Kitaura, S. Noro, *Angew. Chem.* **2004**, *116*, 2388 – 2430; *Angew. Chem. Int. Ed.* **2004**, *43*, 2334 – 2375; c) J. L. C. Rowsell, O. M. Yaghi, *Microporous Mesoporous Mater.* **2004**, *73*, 3 – 14.

[2] H.-C. Zhou, J. R. Long, O. M. Yaghi, *Chem. Rev.* **2012**, *112*, 673 – 674.

[3] a) S. T. Meek, J. A. Greathouse, M. D. Allendorf, *Adv. Mater.* **2011**, *23*, 249 – 267; b) R. J. Kuppler, D. J. Timmons, Q. R. Fang, J. R. Li, T. A. Makal, M. D. Young, D. Q. Yuan, D. Zhao, W. J. Zhuang, H. C. Zhou, *Coord. Chem. Rev.* **2009**, *253*, 3042 – 3066; c) S. Horike, S. Shimomura, S. Kitagawa, *Nat. Chem.* **2009**, *1*, 695 – 704; d) U. Mueller, M. Schubert, F. Teich, H. Puetter, K. Schierle-Arndt, J. Pastre, *J. Mater. Chem.* **2006**, *16*, 626 – 636.

[4] a) K. Sumida, D. L. Rogow, J. A. Mason, T. M. McDonald, E. D. Bloch, Z. R. Herm, T.-H. Bae, J. R. Long, *Chem. Rev.* **2012**, *112*, 724 – 781; b) M. P. Suh, H. J. Park, T. K. Prasad, D.-W. Lim, *Chem. Rev.* **2012**, *112*, 782 – 835; c) H. Wu, Q. Gong, D. H. Olson, J. Li, *Chem. Rev.* **2012**, *112*, 836 – 868; d) G. Férey, C. Serre, T. Devic, G. Maurin, H. Jobic, P. L. Llewellyn, G. De Weireld, A. Vimont, M. Daturi, J.-S. Chang, *Chem. Soc. Rev.* **2011**, *40*, 550 – 562; e) L. J. Murray, M. Dinca, J. R. Long, *Chem. Soc. Rev.* **2009**, *38*, 1294 – 1314; f) S. S. Han, J. L. Mendoza-Cortes, W. A. Goddard IIII, *Chem. Soc. Rev.* **2009**, *38*, 1460 – 1476.

[5] a) J.-R. Li, J. Sculley, H.-C. Zhou, *Chem. Rev.* **2012**, *112*, 869 – 932; b) J.-R. Li, R. J. Kuppler, H.-C. Zhou, *Chem. Soc. Rev.* **2009**, *38*, 1477 – 1504.

[6] a) M. Yoon, R. Srirambalaji, K. Kim, *Chem. Rev.* **2012**, *112*, 1196 – 1231; b) A. Dhakshinamoorthy, M. Alvaro, H. Garcia, *Catal. Sci. Technol.* **2011**, *1*, 856 – 867; c) J. Lee, O. K. Farha, J. Roberts, K. A. Scheidt, S. T. Nguyen, J. T. Hupp, *Chem. Soc. Rev.* **2009**, *38*, 1450 – 1459; d) D. Farrusseng, S. Aguado, C. Pinel, *Angew. Chem.* **2009**, *121*, 7638 – 7649; *Angew. Chem. Int. Ed.* **2009**, *48*, 7502 – 7513.

[7] a) Y. Cui, Y. Yue, G. Qian, B. Chen, *Chem. Rev.* **2012**, *112*, 1126 – 1162; b) L. E. Kreno, K. Leong, O. K. Farha, M. Allendorf, R. P. Van Duyne, J. T. Hupp, *Chem. Rev.* **2012**, *112*, 1105 – 1125; c) C. Wang, T. Zhang, W. Lin, *Chem. Rev.* **2012**, *112*, 1084 – 1104; d) J. Rocha, L. D. Carlos, F. A. A. Paz, D. Ananias, *Chem. Soc. Rev.* **2011**, *40*, 926 – 940; e) M. D. Allendorf, C. A. Bauer, R. K. Bhakta, R. J. T. Houk, *Chem. Soc. Rev.* **2009**, *38*, 1330 – 1352.

[8] a) W. Zhang, R.-G. Xiong, *Chem. Rev.* **2012**, *112*, 1163 – 1195; b) M. Clemente-León, E. Coronado, C. Martí-Gastaldo, F. M. Romero, *Chem. Soc. Rev.* **2011**, *40*, 473 – 497; c) M. Kurmoo, *Chem. Soc. Rev.* **2009**, *38*, 1353 – 1379.

[9] P. Horcajada, R. Gref, T. Baati, P. K. Allan, G. Maurin, P. Couvreur, G. Férey, R. E. Morris, C. Serre, *Chem. Rev.* **2012**, *112*, 1232 – 1268.

[10] M. Eddaoudi, J. Kim, N. Rosi, D. Vodak, J. Wachter, M. O'Keeffe, O. M. Yaghi, *Science* **2002**, *295*, 469 – 472.

[11] P. Serra-Crespo, E. V. Ramos-Fernandez, J. Gascon, F. Kapteijn, *Chem. Mater.* **2011**, *23*, 2565 – 2572.

[12] F. X. Coudert, C. Mellot-Draznieks, A. H. Fuchs, A. Boutin, *J. Am. Chem. Soc.* **2009**, *131*, 3442 – 3443.

[13] T. Devic, P. Horcajada, C. Serre, F. Salles, G. Maurin, B. Moulin, D. Heurtaux, G. Clet, A. Vimont, J. M. Greneche, B. Le Ouay, F. Moreau, E. Magnier, Y. Filinchuk, J. Marrot, J. C. Lavalley, M. Daturi, G. Férey, *J. Am. Chem. Soc.* **2010**, *132*, 1127 – 1136.

[14] S. Biswas, T. Ahnfeldt, N. Stock, *Inorg. Chem.* **2011**, *50*, 9518 – 9526.

[15] J. P. S. Mowat, V. R. Seymour, J. M. Griffin, S. P. Thompson, A. M. Z. Slawin, D. Fairen-Jimenez, T. Duren, S. E. Ashbrook, P. A. Wright, *Dalton Trans.* **2012**, *41*, 3937 – 3941.

[16] Q. Yang, A. D. Wiersum, P. L. Llewellyn, V. Guillerm, C. Serre, G. Maurin, *Chem. Commun.* **2011**, *47*, 9603 – 9605.

[17] F. Vermoortele, M. Vandichel, B. Van de Voorde, R. Ameloot, M. Waroquier, V. Van Speybroeck, D. E. De Vos, *Angew. Chem.* **2012**, *51*, 4887 – 4890.

[18] M. Tonigold, Y. Lu, A. Mavrandonakis, A. Puls, R. Staudt, J. Moellmer, J. Sauer, D. Volkmer, *Chem. Eur. J.* **2011**, *17*, 8671 – 8695.

[19] K. Leus, I. Muylaert, M. Vandichel, G. B. Marin, M. Waroquier, V. Van Speybroeck, P. Van der Voort, *Chem. Commun.* **2010**, *46*, 5085 – 5087.

[20] K. Leus, M. Vandichel, Y. Y. Liu, I. Muylaert, J. Musschoot, S. Pyl, H. Vrielinck, G. B. Marin, C. Detavernier, P. V. Wiper, Y. Z. Khimyak, M. Waroquier, V. Van Speybroeck, P. Van der Voort, *J. Catal.* **2012**, *285*, 196 – 207.

[21] M. Vandichel, K. Leus, P. Van der Voort, M. Waroquier, V. Van Speybroeck, *J. Catal.* **2012**, *294*, 1 – 18.

[22] K. Barthelet, J. Marrot, D. Riou, G. Ferey, *Angew. Chem.* **2002**, *114*, 291 – 294; *Angew. Chem. Int. Ed.* **2002**, *41*, 281 – 284.

[23] V. Van Speybroeck, J. Van der Mynsbrugge, M. Vandichel, K. Hemelsoet, D. Lesthaeghe, A. Ghysels, G. B. Marin, M. Waroquier, *J. Am. Chem. Soc.* **2011**, *133*, 888 – 899.

[24] Y. Zhang, W. Pan, W. Yang, *J. Chem. Phys.* **1997**, *107*, 7921 – 7925.

[25] C. Hansch, A. Leo, R. W. Taft, *Chem. Rev.* **1991**, *91*, 165 – 195.

[26] R. W. Taft, *J. Am. Chem. Soc.* **1952**, *74*, 3120 – 3128.

[27] A. D. Becke, *J. Chem. Phys.* **1988**, *88*, 2547 – 2553.

[28] T. C. Lillestolen, R. J. Wheatley, *Chem. Commun.* **2008**, 5909 – 5911.

[29] F. L. Hirshfeld, *Theor. Chim. Acta* **1977**, *44*, 129 – 138.

[30] P. Bultinck, C. VanAlsenoy, P. W. Ayers, R. Carbó-Dorca, *J. Chem. Phys.* **2007**, *126*, 144111.

[31] T. Verstraelen, P. W. Ayers, V. Van Speybroeck, M. Waroquier, *J. Chem. Theory Comput.* **2013**, *9*, 2221 – 2225.

[32] a) G. Kresse, J. Furthmüller, *Phys. Rev. B* **1996**, *54*, 11169 – 11186; b) G. Kresse, J. Furthmüller, *Comput. Mater. Sci.* **1996**, *6*, 15 – 50; c) G. Kresse, J. Hafner, *Phys. Rev. B* **1993**, *47*, 558 – 561; d) G. Kresse, J. Hafner, *Phys. Rev. B* **1994**, *49*, 14251 – 14269.

[33] a) J. P. Perdew, K. Burke, M. Ernzerhof, *Phys. Rev. Lett.* **1996**, *77*, 3865 – 3868; b) J. P. Perdew, K. Burke, M. Ernzerhof, *Phys. Rev. Lett.* **1997**, *78*, 1396 – 1396.

[34] S. Grimme, *J. Comput. Chem.* **2006**, *27*, 1787 – 1799.

[35] P. E. Blöchl, *Phys. Rev. B* **1994**, *50*, 17953.

[36] B. A. De Moor, A. Ghysels, M. F. Reyniers, V. Van Speybroeck, M. Waroquier, G. B. Marin, *J. Chem. Theory Comput.* **2011**, *7*, 1090 – 1101.

[37] T. Kerber, M. Sierka, J. Sauer, *J. Comput. Chem.* **2008**, *29*, 2088 – 2097.

[38] a) A. D. Becke, *J. Chem. Phys.* **1993**, *98*, 5648 – 5652; b) C. T. Lee, W. T. Yang, R. G. Parr, *Phys. Rev. B* **1988**, *37*, 785 – 789.

[39] P. J. Hay, W. R. Wadt, *J. Chem. Phys.* **1985**, *82*, 270 – 283.

[40] A. Ghysels, T. Verstraelen, K. Hemelsoet, M. Waroquier, V. Van Speybroeck, *J. Chem. Inf. Model.* **2010**, *50*, 1736 – 1750.

[41] a) A. Ghysels, D. Van Neck, M. Waroquier, *J. Chem. Phys.* **2007**, *127*, 164108; b) A. Ghysels, V. Van Speybroeck, T. Verstraelen, D. Van Neck, M. Waroquier, *J. Chem. Theory Comput.* **2008**, *4*, 614 – 625; c) A. Ghysels, V. Van Speybroeck, E. Pauwels, D. Van Neck, B. R. Brooks, M. Waroquier, *J. Chem. Theory Comput.* **2009**, *5*, 1203 – 1215.

[42] M. Vandichel, D. Lesthaeghe, J. Van der Mynsbrugge, M. Waroquier, V. Van Speybroeck, *J. Catal.* **2010**, *271*, 67 – 78.

[43] T. Verstraelen, V. Van Speybroeck, M. Waroquier, *J. Chem. Inf. Model.* **2008**, *48*, 1530 – 1541.

Received: March 26, 2014
Published online on ■■ ■■, 0000

M. Vandichel, S. Biswas, K. Leus, J. Paier, J. Sauer, T. Verstraelen, P. Van Der Voort,* M. Waroquier,* V. Van Speybroeck**

■■ – ■■

Catalytic Performance of Vanadium MIL-47 and Linker-Substituted Variants in the Oxidation of Cyclohexene: A Combined Theoretical and Experimental Approach

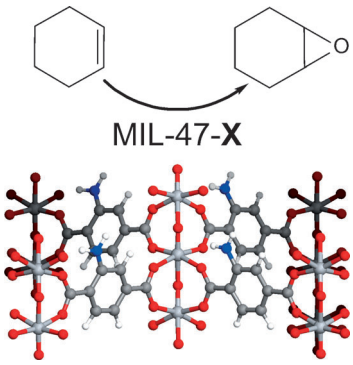

A framework for catalysis: The epoxidation of cyclohexene has been studied on functionalized versions of the metal–organic framework MIL-47 containing V^{+IV} sites. All the investigated substituted MIL-47-X frameworks (X = NH_2, CH_3, F, Cl, Br, OH; see figure) led to an increased conversion to cyclohexene oxide. A linear free-energy relationship was found between centers.